Eur. Phys. J. A **2**, 179–191 (1998)

THE EUROPEAN PHYSICAL JOURNAL A

Fission of highly excited fragments from collisions of 750 A.MeV ^{238}U-ions on ^{208}Pb

W. Schwab[1,2], M. Bernas[2], P. Armbruster[1], S. Czajkowski[1,3], Ph. Dessagne[4], C. Donzaud[1,2], H. Geissel[1], A. Heinz[1,6], C. Kozhuharov[1], C. Miehé[4], G. Münzenberg[1], M. Pfützner[1,5], C. Stéphan[2], K. Sümmerer[1], L. Tassan-Got[2], B. Voss[1,6]

[1] Gesellschaft für Schwerionenforschung, Planckstr. 1, D-64291 Darmstadt, Germany
[2] Institut de physique nucléaire d'Orsay, IN2P3-CNRS, BP 1, F-91400 Orsay, France
[3] Centre d'Etude Nucléaire de Bordeaux-Gradignan, IN2P3-CNRS, BP 120, F-33175 Gradignan, France
[4] Institut de Recherches Subatomiques, IN2P3-CNRS BP 28, F-67037 Strasbourg, France
[5] Instytut Fizyki Doświadczalnej, Uniwersytet Warszawski, Hoża 69, PL-00681 Warszawa, Poland
[6] Institut für Kernphysik, Technische Universität Darmstadt, Schlossgartenstr. 9, D-64289 Darmstadt, Germany

Received: 26 January 1998 / Revised version: 16 March 1998
Communicated by V. Metag

Abstract. Fragments of relativistic 750 A.MeV U-projectiles were investigated by using the fragment separator FRS for magnetic selection of reaction products including ray-tracing and ΔE-ToF techniques. For elements between Ge and Sb, measurements of isotopic yield distributions and velocities revealed three processes: fragmentation, low-energy fission, and high-energy fission. The last of these regimes is presently reported. First and second moments of distributions of mass numbers, atomic numbers and velocities of the corresponding fragments allowed us to identify $^{101}_{43}Tc_{56}$ as the most probable fragment of a high energy symmetric fission reaction. Moreover, we could deduce a hypothetical mean fissioning fragmentation product ^{208}Rn and its highly excited pre-fragmentation parent ^{227}Ra produced in a primary abrasion reaction at an excitation energy of about 290 MeV.

PACS. 25.85.-w Fission reactions – 25.75.-q Relativistic heavy-ion collosions

1 Introduction

"More than fifty years after the discovery of nuclear fission the dynamics of the division of a nucleus into two parts is still one of the most interesting processes of collective flow of nuclear matter and an ideal example for the yet unresolved nuclear many body problem." This sentence, formulated at the 50^{th} anniversary of fission by D. Hilscher and H. Rossner [1] remains a reality.

We investigated the fission of excited nuclei, produced by U-projectile-fragmentation, by measuring systematically the isotopic cross sections for all reaction products identified kinematically. The fission fragments observed stem from different parent nuclei, and their excitation energies vary in a broad range. Nonetheless, high-energy and low-energy fission processes can be unraveled experimentally, since they lead to distinctly different A/Z ratios of the corresponding fission fragments.

More than thirty years ago, after irradiation of uranium targets with proton beams, fission of highly excited nuclei was investigated by radiochemical methods [2] and physical methods [3]. Later, the isotopic yields of Rb and Cs were measured by means of on-line mass-spectrometry techniques [4], followed by a comparative study of (p+U) and (C+U) collisions in the early eighties [5,6]. More recently, studies of fission of excited nuclei were also carried out by means of fusion-fission reactions with heavy ion beams from cyclotrons and tandem accelerators [1,7]. The fusion process leads indeed to a number of intermediate isotopes, the time scale for fusion, however, differs from that for spallation. Note that large angular momenta and collective effects are of importance in fusion, whereas this does not hold for spallation.

The distribution of the mass yields in spallation reactions showed two peaks: a narrow one at large A/Z values, with position and shape independent of the proton incident energy, and—at a lower A/Z value—a second broader peak, which became broader and less intense when the proton energy increased. This second peak was assigned to fission of excited fragments, the presence of which should reflect the onset of particle evaporation. A UCD-like (unchanged-charge division) fission was assumed, which preserves the mass-to-charge ratio (A/Z) of the fissioning nucleus. Further assumptions were that the excitation energy would be transferred to the fission fragments proportionally to their mass and that, after scission, the fragments would undergo neutron evaporation. The remaining question was why the peak of the neutron-rich nuclei stayed centered at a fixed (A/Z) value when increasing the excitation energy, whereas the second peak

was shifting towards the neutron deficient side of the stability valley.

In the present work, this longstanding open question is revisited using new experimental techniques. Other sensitive related questions touched in the paper are: the fission time scales [1,8], the fragmentation of heavy isotopes [9], and the fission of uninvestigated nuclei produced by projectile fragmentation [10,11]. Here, especially the high fission probabilities of spherical nuclei around N=126 are poorly understood [12,13]

After collisions of U-projectiles at relativistic energies with fixed targets, fragments—produced in inverse kinematics—were separated and momentum analysed with the fragment separator (FRS) furnished with additional in-flight identification techniques [14] . The nature of the original process is revealed by the kinematics of the reactions and by the mass distribution of the measured fragments: Collisions at large impact parameters lead to Coulomb fission and low-energy nuclear fission, which are characterized by an asymmetric mass distribution, large neutron excess of the fission fragments, odd-even and shell effects in the mass and energy distributions [15,16]. Less peripheral collisions lead to abrasion of nucleons from the U-projectiles, leaving an excited residual nucleus, which cools down by particle emission and/or fission. The final products of the abrasion-ablation process are referred to as *projectile fragmentation products* or *fragmentation products* throughout the paper. Note that a large fraction of these residual nuclei (appr. 2/3) survives without fissioning [17]. In this high excitation energy regime, the shell effects are wiped out, and the fission yields become mass-symmetric. At even lower impact parameters, the abraded zone increases and the residual fragment is too light, or the fission barrier too high, for fission to occur. The nucleus cools down by particle emission and finally ends in the corridor of neutron-deficient nuclei, where the proton and the neutron separation energies become equal [18,19]. These fragmentation products, far from the projectile, are for the first time effectively separated from the fission fragments due to their distinctly different reaction kinematics.

2 Experiment

Technics used for the separation and identification of fragments produced in collisions of relativistic U-projectiles bombarding a Pb-target with the fragment separator FRS were reported previously [20–23]. The FRS characteristics and the reaction kinematics are recalled briefly in order to illustrate the method applied to distinguish fission fragments from projectile fragmentation products.

2.1 Experimental setup

The U-beam, delivered by the heavy ion synchrotron, SIS, at an energy of 750 A·MeV (β=0.83) and with an intensity of $5{\cdot}10^5$ ions/s was monitored by a secondary electron detector and focussed on a lead target of 1.26 g/cm^2 thickness. Fragments (both fission as well as projectile fragmentation products) emitted within an angular aperture of 30 mrad and a momentum window of 2% are transmitted and analyzed in momentum by the FRS. Note that at velocities of 80% of the speed of light the atomic charge state of the studied elements (from Ge to Sb) is equal to the atomic number Z of the fragments (i.e. A/q = A/Z). With the first two dipole stages, the fragments are momentum selected and their position in the intermediate focal plane is monitored with a position sensitive plastic scintillator counter S_1. When tuned achromatically, the last two dipoles focus each isotope onto a position close to the second scintillator, S_2. The selected ions are Z-identified by their energy loss, ΔE, in a multiply sampling ionization chamber (MUSIC), the four sections of which are position sensitive (via measurement of the drift time in every section). From this, the angle between the trajectory and the optical axis was deduced. The time of flight, ToF, between S_1 and S_2 was measured by the two plastic scintillator counters, the distance between S_1 and S_2 being 37 m. The precise length of the flight path and the value of the effective radius of curvature were calculated from the positions in the two scintillators and the angle of the trajectory. The value of $\beta = v/c$ and γ, the Lorentz factor, were then deduced, and the mass A was obtained from the relation

$$B\rho = 3.107\beta\gamma A/Z \;\; Tm$$

Thus, event-by-event, the atomic number Z, the mass number A, and the $\beta\gamma$-value were obtained from the analysis of ΔE, ToF and Bρ. The resolutions amounted to ΔA/A = 1/250, ΔZ/Z = 1/120 and $\Delta\beta\gamma$ / $\beta\gamma$ = 2.10^{-3}.

2.2 Kinematics of projectile fission

The fission kinematics at relativistic energy has been described in [20] and [21]. The momentum of the emitted fragment in the laboratory results from the Lorentz addition of projectile momentum and of the center of mass (c.m.) fission momentum. The resulting vector lies in a cone ending on an ellipsoidal shell. The thickness of the shell is given by the standard deviation of the velocity distribution of the fission fragments. This momentum phase space is truncated by the angular and momentum acceptances of the FRS as pictured in Fig. 1 for Pd fragments. Only fission fragments emitted forward and backward in the projectile frame are accepted by the FRS aperture. A further restriction is given by the momentum acceptance of the FRS of Δp/p=2%, and forward and backward emitted fragments cannot be transmitted simultaneously since they are apart in the longitudinal momentum by $\approx$ 9%.

For fission at low excitation energy the transmission of fragments through the FRS was evaluated under the assumption that, in the U-center of mass, the fission fragment velocity defined for each element is the same as in thermal-neutron induced fission of ^{235}U. A Monte-Carlo simulation, which includes atomic interactions with matter, was used to calculate the transmission through the

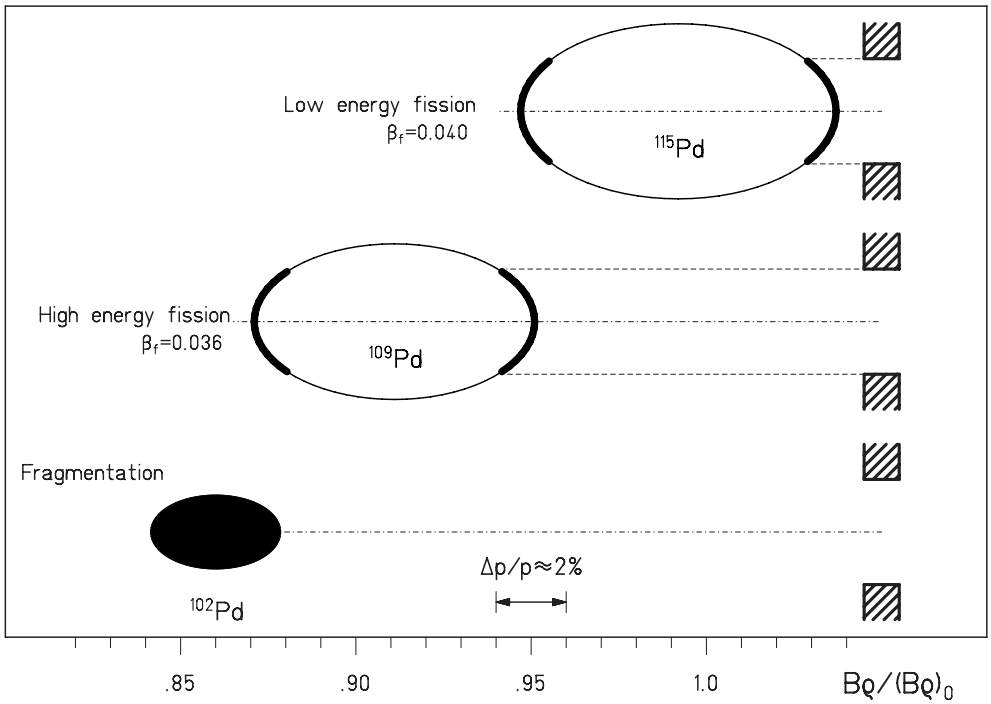

Fig. 1. Momentum phase space of fragments from relativistic ^{238}U projectiles ($\beta = 0.83$) colliding with Pb target nuclei. The mass values given correspond to maximum yields of Pd isotopes for each of the processes. On top (Low energy fission) L.F.: forward or backward emitted fragments with their large relative momentum gap (11% for Pd isotopes) are selected by the angular and momentum acceptances of the FRS. Middle (High energy fission) H.F.: fission of excited fragments leads to less n-rich isotopes and thus the momenta of fragments are reduced. The shrinked ellipse is shifted down. Below: for fragmentation the statistical momentum transfer in all directions produces momenta filling the volume of a small ellipse shown here for light Pd isotopes

FRS [24]. The transmission varies between 1.7% for Ge and 4.5% fot Sb. The anisotropy of the angular distribution in the center of mass system is negligible, since the angular momentum transfer in the reaction has been shown to be smaller than $\Delta l \approx 8\hbar$ [25].

At smaller impact parameters, where nuclear collisions occur, one or more nucleons are abraded from the U-projectile. The residual projectile fragmentation product is usually not produced in its ground state but in an excited one. This fragmentation product releases a fraction of its excitation energy by the emission of nucleons, mainly neutrons. Near the end of the deexcitation process the residual nucleus undergoes fission, and finally a few more neutrons are emitted by the fission-fragments. The final fission fragments are, thus, less neutron-rich than those from low-energy fission. The total kinetic energy of fission (TKE) for a fissioning species stays almost constant at rising excitation energy [16]. Therefore the fragment momenta are lower, in the laboratory system, since the mass is smaller. It is illustrated in the middle part of Fig. 1, where the ellipse shrinks (with respect to the low energy fission in the uppermost part of the fig.) and is shifted to the left, i.e. towards smaller magnetic rigidities.

The lowermost part of Fig.1 illustrates the momentum space filled by projectile fragmentation products for isotopes of the same element, Pd. The velocity of those products is close to the projectile one, but—for a given atomic number—their masses are much lower than those of the fission fragments due to the many neutrons lost in the long cascade of emitted particles. Therefore, their magnetic rigidities are well below the beam rigidity. The solid black ellipse reflects the fact that the $\beta\gamma$ (momenta/mass unit) distribution, populated by the fragmentation process is rather narrow and of a Gaussian type.

2.3 Experimental settings

High energy fission products were observed at Bρ-values smaller than Bρ_0, the stiffness of the beam, in the range $1 >$ Bρ/B$\rho_0 > 0.86$. In this range data were taken at only four magnetic settings. We do not present here the primary (ΔE-$\beta\gamma$) scatter-plots, but we show in Fig. 2 the equivalent scatter-plots (ΔE-A/Z) of fragments transmitted at four rigidities smaller than that of the beam, Bρ/(Bρ)$_0$ = 0.97, 0.94, 0.90 and 0.86. Because of the rather thick Pb target, the selected fragments covered a defined range of velocities $\Delta\beta\gamma/\beta\gamma \approx 4\%$ due to target location straggling effects, and hence a multitude of masses were transmitted simultaneously [20]. For Bρ/(Bρ)$_0$=0.97 and 0.94 two groups of ions transmitted in the same narrow momentum window are clearly distinguished. They are associated with two regimes of neutron excess (or A/Z) and $\beta\gamma$. The group with the largest A/Z ratio and the

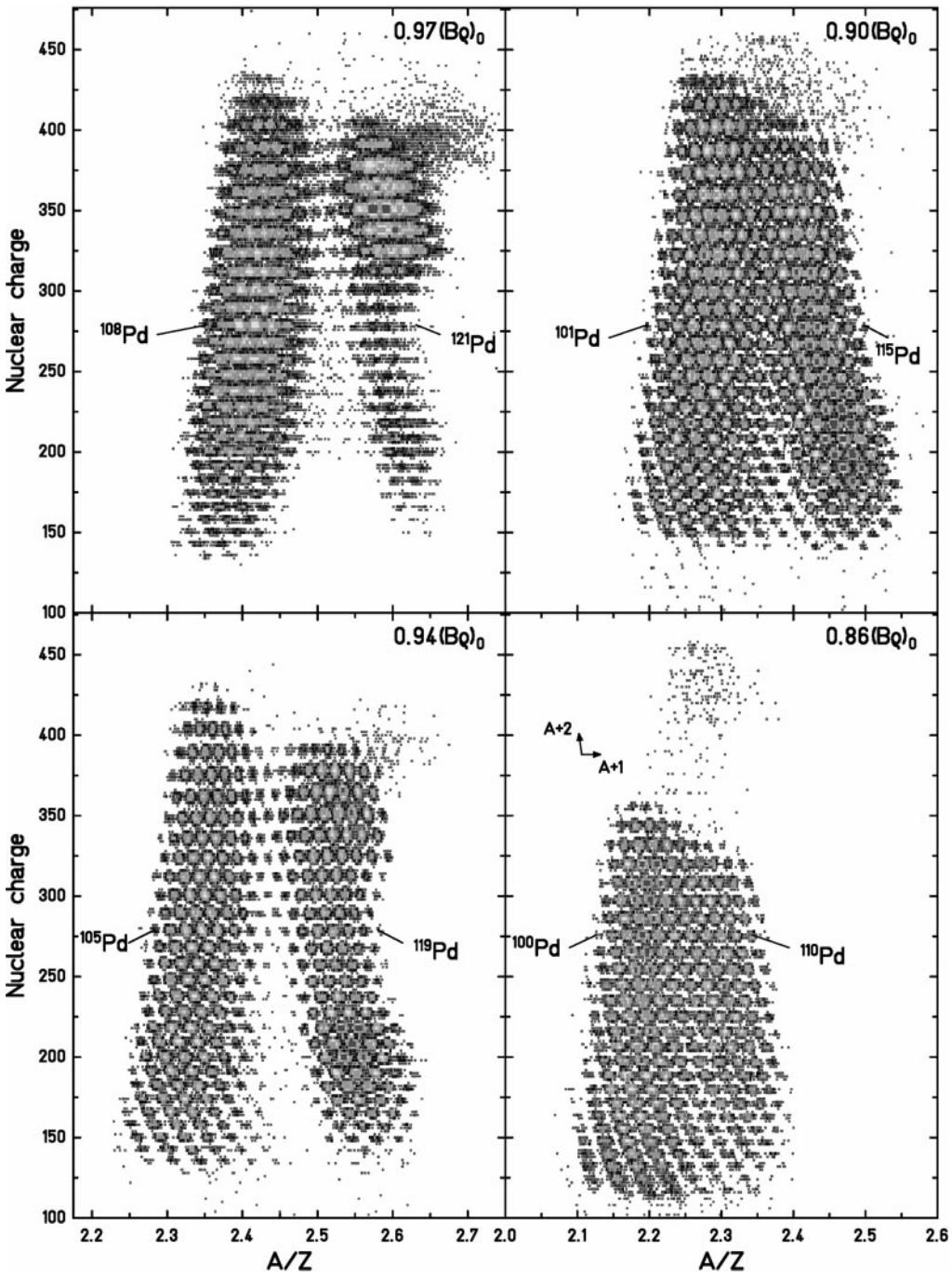

Fig. 2. Scatter plots ΔE versus A/Z of the isotopes transmitted by the FRS at rigidities of 0.97, 0.94, 0.90, 0.86 of the rigidity of projectile $(B\rho)_0$. Two groups of isotopes are transmitted simultaneously, the lower masses coming with larger velocities. Backward low energy fission (BLF) at right on the two upper plots and forward high-energy fission at left (FHF). Backward high-energy fission (BHF) on the right of the lower plots and fragmentation (FR) on the left. The masses of Pd isotopes under scope range between A = 119 and A = 101

characteristic double-humped isotope distribution stands for low-excitation backward-emitted fission products. The two "clouds" of asymmetric fission centered on Zr and Te show up clearly, as observed for forward emitted fragments [22]. The reduction of the rate of light fission products as compared to the heavier, at $B\rho = 0.97$, is due to their larger c.m.-velocities; compared to heavy fragments, light fragments backward emitted are shifted down in momentum as the forward emitted ones are shifted up due to their larger center of mass velocities [21]. At lower A/Z ratio, a second uniform group of fragments comes with a larger velocity, since it comes in the same FRS setting i.e. in the same momentum window. It results from fission fragments of highly excited U-fragmentation products emitted in the

forward direction. The elemental yield reaches its maximum close to Pd as expected for symmetric fission. For $B\rho/(B\rho)_0 = 0.90$ and 0.86, again two groups of isotopes were transmitted. The group with the larger A/Z values corresponds to fragments due to fission of highly excited U-fragmentation products emitted in backward direction. The isotopes at lower A/Z values are direct residues of projectile fragmentation, as pictured on the lowermost part of Fig. 1.

3 Data analysis

The purpose of the analysis is to characterize events due to fission at high-excitation energy and to obtain the production yields for each fragment. The distribution of yields should reveal the properties of the parent fissioning nuclei and their excitation energy. After the A and Z identification of fragments, the Bρ-scanning provides the momentum per mass unit - or $\beta\gamma$ - distributions from which fission and fragmentation products are disentangled.

For each Z value by setting ΔE windows on the scatter-plots of Fig. 2, counting rates for each mass number are obtained. As an example Fig. 3 shows the mass spectra of Pd taken at the four rigidities where measurements were performed. In total 20 different Pd isotopes are seen. Each spectrum shows the production in two mass regions discussed previously on the scatter-plots. At the two highest rigidities, backward-emitted low-energy fission (B.L.F.) fragments analyzed in the work of [22] and forward-emitted high-energy fission (F.H.F) products are transmitted. At the two lowest rigidities, the group of the lightest masses are direct U-fragmentation products. In the region between A=105 and 115, the isotopes are produced by high-energy fission emitted backward (B.H.F). In the overlapping regions (see lower frames of Fig. 3), counting-rates versus masses are fitted by two Gaussian distributions in order to attribute fragments either to fission or to fragmentation.

After normalizing the spectra for the beam intensities and dead times, the data are gathered isotope by isotope for each element as a function of $\beta\gamma$ (Fig. 4). The data points for ^{110}Pd, marked in black on Fig. 3, are shown with full dots on Fig. 4a in order to illustrate the method. In the upper frame one recognizes the two peaks due to the FRS selection of forward and backward fission. They are centered around the $\beta\gamma$ value of the primary beam, 1.41, and separated in momentum by a relative difference of $\Delta\beta\gamma$ / $\beta\gamma \approx 9\%$, as expected for a binary fission process [21]. The yields of the lightest isotopes shown in Fig. 4b are represented by a single Gaussian distribution centered at the $\beta\gamma$-value of the beam as expected from ^{238}U fragmentation. Those last fragments are transmitted through the FRS ten times better than fission products (see bottom of Fig. 1). Their production yields are reported and discussed in a dedicated paper [23].

We focus here on fragments produced by the fission of U-fragmentation products, i.e. on fragments characterized by the double-humped velocity distribution shown in

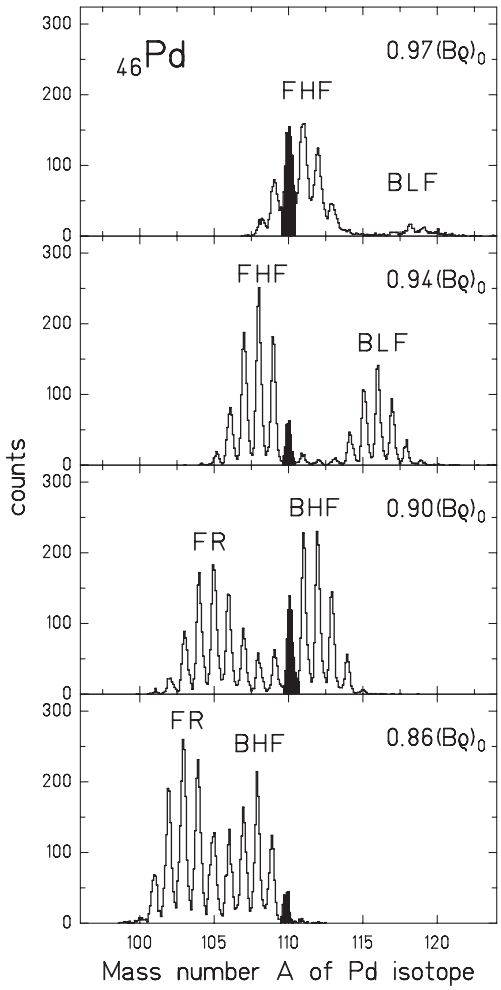

Fig. 3. Mass distributions for Pd obtained by setting ΔE windows on the four scatter-plots shown on Fig. 2. The region populated by forward and backward high-energy fission are indicated by FHF and BHF. In the region of n-deficient isotopes, fragments produced by U-fragmentation (FR) are seen

the upper part of Fig. 4. Even though the number of Bρ-settings is only four, the data analysis is trustworthy due to redundancy given by the numerous isotopes observed per element, each at a slightly different velocity. A few simplifying assumptions are made like in our analysis of fission at low excitation energy:

1) For isotopes of a given element, the distance between the forward and backward peaks (see Fig. 4a) is proportional to the c.m. fission velocity β_f. The fission kinetic energy is mainly due to Coulomb repulsion at scission. To first order β_f varies very slightly with the mass of the isotope. Therefore, $\Delta\beta\gamma$ is assumed to be the same for the isotopes of a given element.

2) The widths, or standard deviations, of the Gaussian-like velocity distributions are governed by the "location straggling" in the target [21], which mainly depends on the atomic number Z. We assume that the widths for isotopes of an element are the same for either backward or forward emission. Distance and width of the two peaks

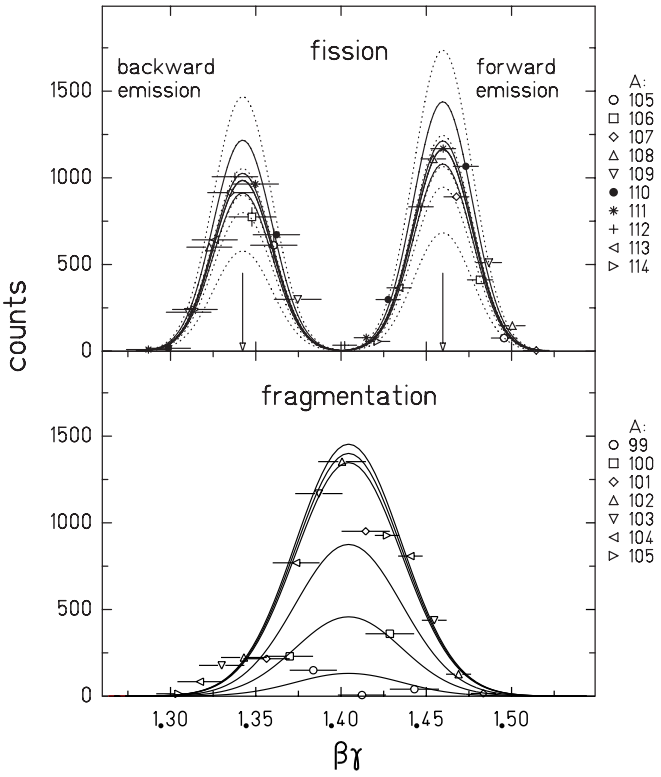

Fig. 4. $\beta\gamma$ distribution of Pd isotopes measured over the four Bρ-settings. The upper part shows the double humped structure associated to forward and backward emitted fission products. The distribution of very neutron-deficient fragments is found to be centered around the beam value of $\beta\gamma$ at 1.41. Those fragments result from fragmentation

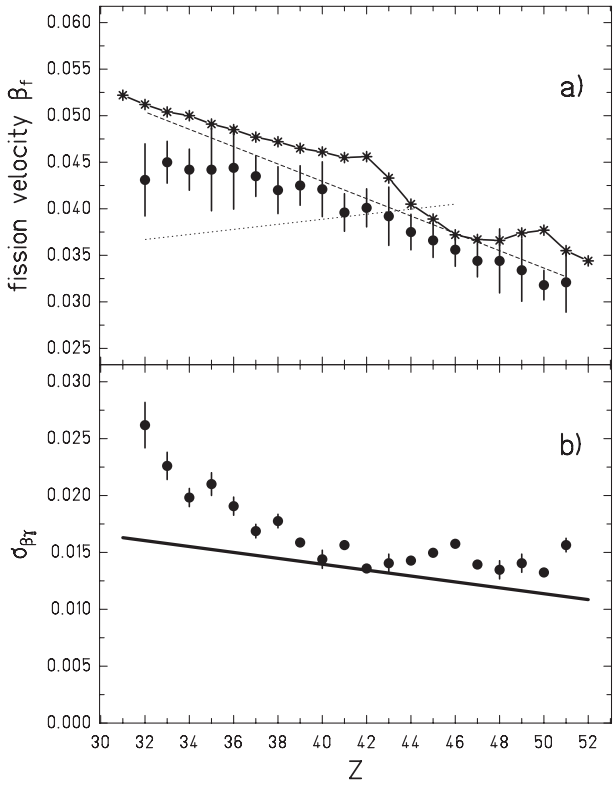

Fig. 5. a Fission fragment velocities as a function of fragment atomic number for the regime of high energy fission. The stars show the values obtained for thermal neutron induced fission. The curves illustrate two extreme assumptions, using the TKE-systematics of Viola [30]: either only one nucleus, ^{208}Rn, is undergoing symmetric fission (dashed line), or fragmentation products, the atomic number of which equals twice the atomic numbers of the observed fission fragment (dotted line), fission symetrically. **b** the standard deviation of the velocity distribution $\sigma_{\beta\gamma}$ as a function of fragment atomic number. The line is the estimated variation due to target location straggling assuming fission of ^{208}Rn

are taken as two free parameters, the same for all isotopes of an element. Their values are given by the fitting procedures together with a normalization for each of the isotopes. When $\beta\gamma$ values are located far on the tail of the Gaussian distributions, the weight of the data points are reduced.

3) Forward-emitted fragments have a larger velocity than backward emitted ones, and they are better transmitted. For a given fragment, the ratio of the transmissions is the ratio of the squares of the velocities $(\beta_0 + \beta_f)^2/(\beta_0 - \beta_f)^2$. This condition is used to constrain the fits.

4 Results

4.1 Velocity of fission fragments in center-of-mass frame

The fission velocity β_f is deduced from the distance between the forward and the backward emitted fission peak. The difference of energy losses in half the target between forward and backward-emitted fragments are negligible, therefore

$$\beta_f = ([\beta\gamma]_+ - [\beta\gamma]_-)/(\gamma_+ + \gamma_-)$$

where β and γ are taken at the target center.

From the $\beta\gamma$ distributions for the different atomic numbers Z, like the one shown in Fig. 4 for palladium, we calculate the mean velocity β_f. It is shown in Fig. 5a as a function of the atomic number of the fragment. The values are found to be rather close to the values known from ^{235}U(n_{th},f). In Fig. 5b the standard deviations $\sigma_{\beta\gamma}$ are shown with the variation expected from target location straggling. The increase of $\sigma_{\beta\gamma}$ with decreasing atomic number is discussed below.

4.2 Isotopic yields

Isotopic yields are obtained by dividing the maxima of the yields, as shown for Pd in Fig. 4a, by the transmission through the FRS. The transmission, calculated by using the simulation program MOCADI [26] and ^{235}U(n_{th},f) fission velocities, is only a function of the atomic number Z and not of the mass A, as discussed before. The reduction of the fission velocities by 5 to 15 %, as compared to

(n_{th},f) fission velocity, Fig. 5a, is taken into account. The transmission grows from 1.9% for Ge up to 4.8% for Sb isotopes. The error bars given on the final yields account for statistical errors and the fluctuations on $\sigma_{\beta\gamma}$ (Fig. 5b), which contribute to the relative errors with about 7%.

Figure 6 shows comprehensive isotopic distributions of the 600 fission fragments for the elements investigated from germanium up to antimony, see Table 1. The neutron-rich isotopes are produced by Coulomb fission and low-energy nuclear fission. The corresponding yields

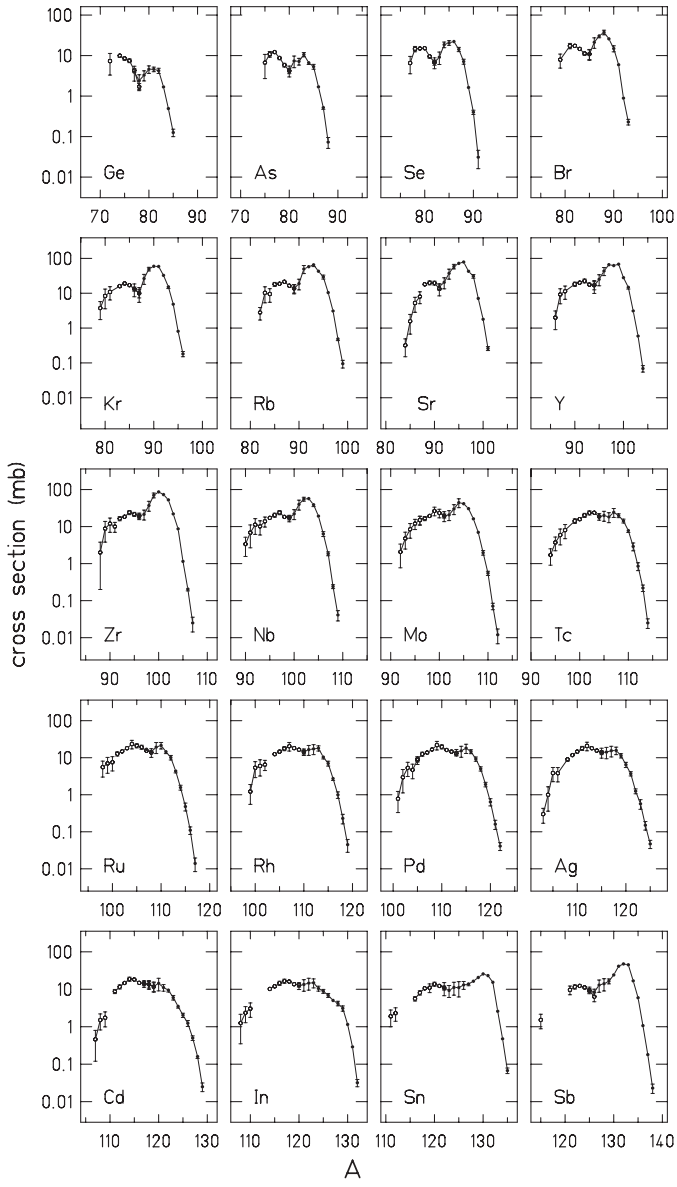

Fig. 6. Fission cross sections are given for both fission regimes, low and high energy fission. The low energy process analyzed in [22] is followed by processes carrying more and more excitation energy and there is a gradual transition between the two regimes. Still a clear maximum is seen also in the second phase. On the left part of the distribution few values are given with large uncertainties. Here fragmentation events are difficult to disentangle from fission events

Table 1. Production cross sections for the isotopes observed in high energy fission events

Z	A	σ/mb	Z	A	σ/mb	Z	A	σ/mb
32	74	10.0(1.0)	39	90	18.4(1.5)	46	105	9.1(1.4)
	75	8.5(0.8)		91	20.1(1.6)		106	12.6(1.6)
	76	7.5(0.8)		92	22.6(2.9)		107	13.7(1.1)
	77	4.3(0.5)		93	17.7(1.5)		108	16.7(1.3)
	78	1.7(0.3)		94	17.0(4.5)		109	21.9(5.7)
							110	19.7(2.5)
							111	16.2(1.2)
							112	14.6(1.1)
							113	13.1(1.7)
33	76	10.9(1.0)	40	92	16.4(2.1)	47	109	11.7(1.0)
	77	12.2(1.1)		93	18.4(1.4)		110	14.6(1.1)
	78	8.7(0.8)		94	24.1(3.1)		111	17.9(2.3)
	79	5.8(0.6)		95	21.5(2.7)		112	20.8(5.4)
	80	4.2(0.6)		96	19.3(2.5)		113	18.0(1.4)
							114	15.6(1.2)
							115	13.9(1.8)
34	78	14.7(1.3)	41	95	17.2(1.3)	48	111	8.8(1.1)
	79	14.9(1.3)		96	20.4(2.6)		112	11.6(1.5)
	80	15.2(1.3)		97	24.0(3.0)		113	14.7(1.1)
	81	9.6(0.9)		98	18.3(1.5)		114	18.7(2.4)
	82	6.8(1.0)		99	17.3(2.2)		115	18.2(1.4)
							116	14.9(1.2)
							117	14.2(1.8)
							118	13.5(3.5)
							119	11.7(3.1)
35	81	17.3(1.4)	42	96	15.0(4.0)	49	114	10.2(0.8)
	82	17.4(1.4)		97	16.5(2.1)		115	12.0(1.0)
	83	14.6(1.2)		98	19.4(1.5)		116	14.6(1.9)
	84	11.2(1.0)		99	26.5(6.9)		117	16.5(2.1)
	85	10.9(2.9)		100	23.3(6.1)		118	16.1(1.2)
				101	19.4(2.5)		119	13.5(1.1)
				102	15.5(5.0)		120	13.1(1.7)
36	83	16.0(1.4)	43	99	14.2(1.1)	50	116	5.6(0.7)
	84	19.1(1.5)		100	15.8(1.2)		117	8.1(1.1)
	85	17.1(1.4)		101	20.2(2.5)		118	10.6(0.9)
	86	13.3(1.8)		102	23.5(3.0)		119	11.0(2.9)
	87	10.0(2.6)		103	23.7(1.8)		120	13.8(1.7)
				104	18.7(1.4)		121	12.3(0.9)
							122	10.9(1.4)
37	85	18.1(2.4)	44	101	12.8(1.6)	51	121	9.7(2.5)
	86	18.7(1.5)		102	14.9(1.1)		122	11.6(1.5)
	87	21.4(1.7)		103	18.1(1.4)		123	12.3(1.0)
	88	16.4(1.4)		104	23.4(6.1)		124	11.2(0.9)
	89	13.7(3.6)		105	21.1(2.7)		125	9.3(1.2)
				106	19.3(2.4)		126	6.3(1.7)
				107	15.5(1.2)			
				108	13.8(3.6)			
38	88	18.0(1.4)	45	104	12.5(1.0)			
	89	20.0(2.5)		105	14.6(1.1)			
	90	19.7(2.5)		106	17.7(2.2)			
	91	13.4(5.0)		107	20.5(5.3)			
				108	18.2(1.4)			
				109	16.4(1.3)			
				110	14.3(1.8)			

were analyzed in the work of C. Donzaud et al. [22]. At the other end, on the neutron-deficient side, the few lightest fission products were analyzed together with the fragmentation data [23]. Here a different procedure to evaluate the transmission was used. Between these two extremes, intermediate mass isotopes are observed. For light elements up to Mo and heavy elements Sn and Sb, the predominant peak due to Coulomb and low-energy nuclear fission is rather well separated from a wider peak due to high-energy fission. The total width of the isotopic distributions is increasing with the Z of the fragments. The contribution of high energy fission increases with Z, and close to the mass-symmetry it becomes the main process. Error bars are the largest in the intermediate mass region where the rigidities of the forward emitted fragments and of the U-beam are close, and at the smallest masses, where the contributions of fragmentation and fission overlap.

In order to extract further information for each element, Gaussian distributions are fitted to the high energy fission component of Fig. 6 assuming implicitly a symmetric isotopic distribution. Thus, cross sections σ(Z), standard deviations σ_N^Z, and the mean mass numbers $\overline{A}$ are determined for each element, see Table 2. The mean A/Z values of the fragments are found to slightly and continuously increase from 2.32 to 2.42 with Z varying from 32 to 51. They are smaller than the value of 2.59 for the U-projectile.

Table 2. Most probable mass value for the isotopes of each element observed from high energy fission. The standard deviation, σ_N^Z, (in a.m.u.) and the integrated cross sections per element (in mb) are given

Z	$\overline{A}$	σ_N^Z/a.u.	σ(Z)/mb
32	74.4(4)	2.0(0.3)	49(8)
33	76.3(6)	2.5(0.5)	72(16)
34	78.8(4)	2.4(0.4)	92(14)
35	81.4(7)	2.7(0.9)	121(39)
36	84.2(3)	2.3(0.5)	109(18)
37	86.5(3)	2.6(0.7)	133(33)
38	89.1(3)	2.2(0.9)	113(40)
39	91.5(3)	3.1(1.1)	159(47)
40	94.5(5)	3.1(1.0)	171(49)
41	96.8(3)	3.0(0.9)	158(35)
42	99.5(7)	3.7(1.4)	198(66)
43	102.3(3)	3.3(0.5)	183(23)
44	104.6(2)	3.5(0.5)	176(17)
45	107.3(3)	3.7(0.6)	172(22)
46	109.6(2)	4.0(0.5)	178(15)
47	112.2(2)	3.4(0.5)	157(15)
48	115.0(3)	3.5(0.4)	150(14)
49	117.5(3)	3.7(0.6)	144(18)
50	120.0(3)	3.1(0.4)	102(11)
51	122.9(4)	2.7(0.6)	84(17)

4.3 Isotopic distributions

The peaks associated with the yields of high energy fission, shown in Fig. 6, are integrated and the distribution of elemental cross sections is given in Fig. 7a. The summed cross sections for fragments with a defined number of neutrons N are given in Fig. 7b as a function of N. Both distributions are rather flat and nearly symmetric.

- The element distribution (Fig. 7a) is centered around technetium ($\overline{Z} = 42.9 \pm 0.03$) giving an average number of 6.2 protons released in the process. The FWHM of the element distribution is found to be (16.2 ± 0.9) charge units, slightly more than the value of 14.1 obtained in nuclear-induced fission of a single fragmentation product [11] separated by using the method described in ref [10]. Our width was also found in an experiment from LBL, Berkeley, where Be was irradiated with a 120 A.MeV ^{238}U beam [27].
  For the isotonic yield distributions on Fig. 7b, the mean value of $\overline{N} = 58.1 \pm 0.3$ shows that during the different phases of the reaction, an average number of (29.8 ± 1) neutrons are removed from the primary ^{238}U-nucleus. The higher cross sections for N=(60 ± 1) deviate less than a 2 σ-effect. Further experiments should verify an eventual increase of yields at these neutron-numbers.
- The standard deviations of the isotopic distributions σ_N^Z resulting from the integration of the high energy fission peaks of Fig. 6 are not constant (Table 2 and Fig. 8). They increase from 2 a.m.u. for light elements

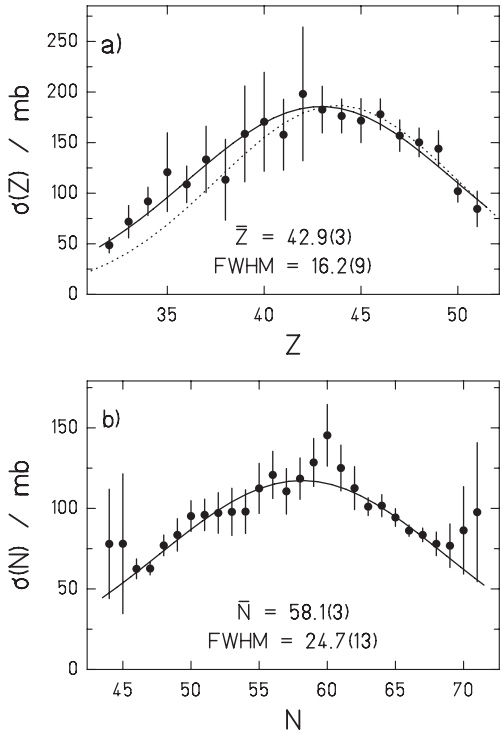

Fig. 7. Integrated **a** elemental, $\sigma(Z)$, **b** isotonic, $\sigma(N)$ cross sections obtained for the fission of fragmentation products. The dashed line is the result of the simulation described in the discussion

Table 3. Parameters characterizing the distribution of high energy fission events in 750 A.MeV ^{238}U on Pb collisions

σ^{tot}/b	E_k/MeV	$\overline{Z}$	$\overline{N}$	$\overline{A}$	σ_Z/a.u.	σ_N/a.u.	σ_A/a.u.	σ_N^Z/a.u.	σ_Z^N/a.u.	$\sigma_{Z,N}^A$/a.u.
1.4 ± 0.2	158 ± 3	42.9 ± 0.3	58.1 ± 0.3	101.0 ± 0.5	6.9 ± 0.7	10.5 ± 1.1	17.2 ± 1.7	3.2 ± 0.7	1.9 ± 0.5	1.3 ± 0.3

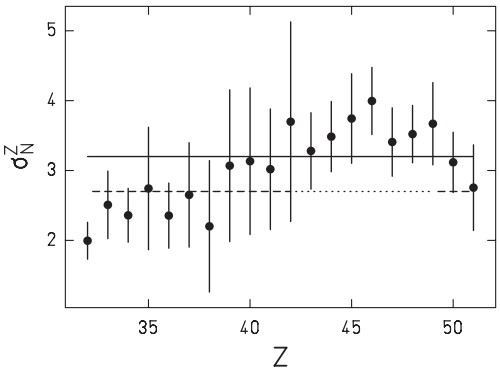

Fig. 8. The local standard deviation of the isotopic distribution σ_N^Z as a function of atomic number. The full line is the weighted mean value. The dashed line is the same excluding the elements in the range Z=42-49

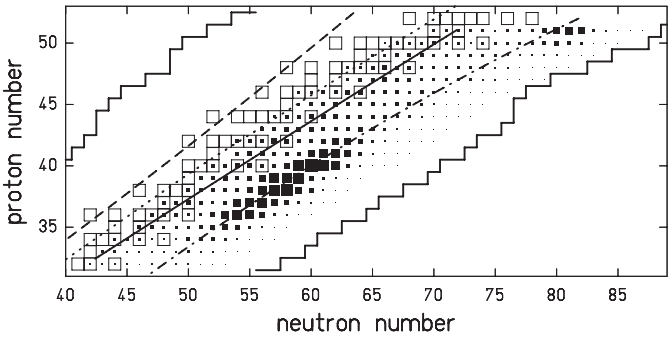

Fig. 9. Region of the nuclear chart populated by the U-fragments of the present study. The limits involve all the observed isotopes including the ones recently detected in U projectile fission on Be-target [33]. The empty squares indicate the stable isotopes, the bottom of the valley of stability being represented by the dotted line. The full square symbols scale the production cross sections as given in table 1 and in ref [22]. The squares cover a range of cross sections between 100 mb and 0.1 mb and change size in increments of 1.5. The full line corresponds to the ridge of the maximum production by fission of projectile fragmentation products, as presented in this paper. The dotted-dashed line symbolizes the maximunm yields of low-energy fission as reported in [22]. The dashed line represents the ridge of maximum production by direct fragmentation [23]

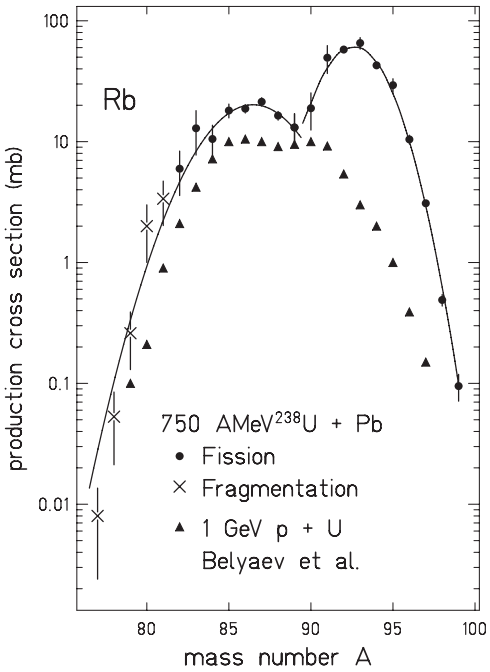

Fig. 10. Total cross sections for production of rubidium isotopes as a function of atomic mass compared to the data obtained in bombarding a U target with 1 GeV protons [5]

up to 4 a.m.u. going from Ge to Cd. Large values are found between Z=42 and 49, i.e. for elements in the low energy fission valley. There, the separation between high energy and low energy fission is less obvious and it may cause the increase of σ_N^Z. Weighting the standard deviations by the elemental yield gives a mean value of (3.2 ± 0.7) a.m.u. Suppressing the elements Z=(42-49) would reduce the mean value to (2.7 ± 0.7) a.m.u.

- The positions of the centroids $\overline{A_{HF}}$ extracted from the fits (Table 2) are compared to the mean values of the mass number $\overline{A_S}$ for stable nuclei, mean values for low energy fission and for fragmentation, see Fig. 9. For all elements $\overline{A_{HF}}$ is found to be larger than $\overline{A_S}$ by about 3 mass units. $\overline{A_{HF}}$ follows the curvature of the valley.
- From both distributions shown on Fig. 7a and 7b, cross sections related to the high energy fission regime are derived. We found (1.6 ± 0.2) b, which confirms the value of (1.4 ± 0.2) b obtained in an independent direct measurement [17].
- Figure 10 shows the complete set of cross sections for rubidium isotopes from Coulomb and low energy nuclear fission, high-energy fission, and fragmentation. The few data from fragmentation do not contribute much to the elemental yield and do not change significantly the parameters of the distribution, as seen by comparing the Rb distribution of Fig. 6 with the complete distribution in Fig. 10. This element is selected since results can be compared with previous data obtained with on-line mass separator techniques by Belyaev et al. [5] for the p+U system at 1 GeV. For the two experiments having separated the two fission

regimes, we find, that the yields for low energy fission processes are enhanced by a factor of 20 in the (U + Pb)-system as compared to the (p+U)-system, and by a factor of 2 for high energy fission. The value of $\overline{A_{HF}}$ = 86.5 found in our experiment for Rb (see Table 2) agrees with the corresponding value derived from the (p+U) experiment. The small ratio of cross sections, a factor 2, is remarkable in regard to the large total energy available and the larger interaction radius of the (Pb + U)-system. Protons are very effective projectiles, not only their beams are the strongest, but also production cross sections of up to 10 mb are surprisingly large.

Table 3 summarizes the most important numbers derived from our results on the high energy fission of fragmentation products.

5 Discussion

During the abrasion phase, the average ratio of the number of protons versus the number of neutrons removed from the U-projectile is equal to Z_u/N_u. The residual hot fragment deexcites by emission of many neutrons and a few protons, as the proton has to pass the Coulomb barrier. Besides the difference of energies needed for emitting protons and neutrons, the ratio of protons/neutrons is governed by the total excitation energy available and by the level densities in the final states. Along the evaporation cascade, down to an excitation energy of about 40 MeV, where fission is likely to occur [1], many nucleons, mostly neutrons, are emitted. Finally, additional neutrons are freed from excited fission fragments.

From the present restricted experimental information we can build a simplified scenario of the process. We reconstruct the mean highly excited parent-fragment (A^*, Z^*), its excitation energy E^*, as well as the fissioning nucleus (A_0, Z_0), which gives rise to the most probable fission fragments observed.

5.1 Reconstruction of the mean deexcitation chain

Assuming a final symmetric fission, a hypothetical parent nucleus is reconstructed from the average proton and neutron numbers observed for the final fragments (see Fig. 7). There are 85.8 protons and 202 nucleons found in the most probable pair of fission fragments. In the complex series of processes leading finally to a pair of ^{101}Tc fragments, altogether 36 nucleons are released. As nucleon balance we find that during the nuclear collision 6.2 protons and 29.8 neutrons were abraded or emitted from ^{238}U.

A primary abrasion stage heats the ^{238}U nucleus. The ratio of abraded protons π_{abr} to neutrons ν_{abr} should be proportional to the Z_u/N_u ratio in the mother nucleus, 92/146. 27 MeV are invested for each abraded nucleon [28]. The primary fragment cools down by evaporation of a few protons π_{evap} and of a large number of neutrons ν_{evap}. The evaporation process is governed by the effective separation energies for protons and neutrons and the mean energy where fission occurs.

The average energy to evaporate a proton is estimated from $e_p = S_{2p}/2 + B_p^{eff} + 2T$ with B_p^{eff} an effective Coulomb barrier, T the temperature and S_{2p} the two nucleon binding energy [23,28]. In the following a value of e_p of 20 MeV, averaged over the evaporation cascade, is used. To free a neutron, the averaged energy $e_n = S_{2n}/2+2T$ is assumed to be 12 MeV. When neutron evaporation times approach the time to overcome the fission saddle point the competition with fission sets in [29]. The angular momentum of the excited nucleus is rather low, thus we are using the l=0 fission barriers. The fragment having a liquid-drop fission barrier of 7 MeV is assumed to fission at an excitation energy of 40 MeV. Each neutron emitted from a fission fragment carries away about 9 MeV. Four neutrons are assumed to be emitted by excited fission fragments. In addition, symmetric fission at the barrier releases two more neutrons. These neutron take their energy out of the fission energy and do not contribute to the energy balance. The total of 6 neutrons accompanying fission is consistent with the findings in [1].

From energy and particle conservation, with the parameters given, the mean number of abraded particles (ν_{abr} = 6.6 and π_{abr} = 4.2) and the energy transfer of (291 ± 17) MeV are determined. The most probable primary nucleus produced by fragmentation and leading to fission would be ^{227}Ra. This hot nucleus would evaporate a mean number of 17.5 neutrons and of 2 protons in an evaporation cascade carrying away 251 MeV and leading to $^{208}_{86}$Rn$_{122}$. This nucleus would then undergo fission at 40 MeV excitation energy emitting the above 6 post-scission neutrons and ending up in a pair of ^{101}Tc.

5.2 Velocity of fission fragments and total kinetic energies

The velocity measurement gives for the hypothetical nucleus ^{208}Rn a TKE of (158 ±3) MeV in agreement with the systematics of Viola [30]. When splitting into fragment pairs of total charge Z_0 = 86, ^{208}Rn releases two fragments distributed around the symmetric breaking, the velocity of which, because of momentum conservation, increases with decreasing atomic number Z_L. The c.m. velocity β_L is calculated from $\beta_L = 3.29(Z_0/2\text{-}Z_L)/A_0^{2/3}$. This dependence is shown on Fig. 5a by the dashed line. The slope follows nicely the experimental values down to Z_L/Z_H = 36/51. For the lightest fission fragments, however, the measured velocities are smaller and indicate that the fragments could come from fission of nuclei with Z<86. In another working hypothesis we assume that a series of parent nuclei with atomic numbers Z_0 = 2Z, Z being the atomic number of the observed fragment, are involved. The dotted line in Fig. 5 shows the distribution of velocities expected in this case. The mass values of the fissioning systems are reconstructed from the values given in Table 2 and with ν_f = 6. The velocities slightly decrease when going from $Z_0/2$ = 46 to $Z_0/2$ = 32. As a conclusion, the presence of fissioning nuclei with Z < 86 contribute to

decrease the mean velocity of the fission fragments, as observed experimentally. The deviation in the region $Z_L < 36$ can be explained by the increasing contribution of different parent nuclei. Moreover, the difference between $\sigma_{\beta\gamma}$ calculated from target location straggling and observed experimentally, see Fig.5b, could also be attributed to a contribution of different sources which increases with decreasing Z.

5.3 Yields distributions

The yield distributions of all nuclei observed in hot fission span an extended, flat ridge defined at a given element by the isotope of maximum yield (table 2). Two local parameters describe the width of the distribution in the N, Z plane (Fig. 9). On the ridge of the most abundant fission products, the local widths of the primary proton, neutron and mass yields are related to the charge density Z_0/A_0 of the fissioning nucleus by the principle of unchanged charge density (UCD), $Z_{ucd} = Z_0$ (A' / A_0) with A' the mass of the fission product before it cooled down by neutron emission. The isotopic yields for a given element and the isotonic yields for a fixed neutron number are related as $Y^Z/Y^N = N_0/Z_0$. The standard deviations of the local charge distribution σ_Z^N and σ_Z^A at constant N and A and the corresponding value of the neutron distribution σ_N^Z at constant Z fullfill the relations $A_0\ \sigma_Z^A = N_0\ \sigma_Z^N = Z_0\ \sigma_N^Z$. These relations which follow from the UCD principle and the geometry of the nuclear yield distribution in the N, Z plane allow to connect the different presentations of the yields and standard deviations assuming smooth primary-yield distributions. They would break down in case of sudden irregularities of the surface. They do not take into account known small deviations from the UCD rule, nor rapid local changes in the pattern of evaporated neutrons and odd-even effects introduced by the nuclear structure of fission fragments.

In low-energy fission, a mass distribution Y(A) and a local isobaric width parameter σ_Z^A were used to describe the mass yields [15]. We choose here to plot the yield distributions Y^Z(N) and Y^N(Z), Fig. 7, and the local standard deviation σ_N^Z, Fig. 8. The distribution for a given element involves the highest number of isotopes and therefore provides a more reliable extraction of the fit parameters. The weighted mean value obtained, $\sigma_N^Z = (3.2 \pm 0.7)$ a.m.u., is much larger than in low-energy fission [22]. The charge polarization -or isospin- degree of freedom characterized by the mean value $\sigma_Z^A = (Z_0/A_0)\sigma_N^Z = 1.3$, with Z_0 and A_0 referring to the fissioning nucleus, is softened by a factor of 2.5, as compared to thermal-neutron fission where $\sigma_Z^A = 0.53$ [15]. Omitting the elements in the valley, see Fig. 8, the softening would still be a factor of 2.1.

The mean values of the parameters characterizing the fissioning nucleus are deduced from the mean number of protons and neutrons of the fission fragments, but the actual distribution of fission fragments results from many different parent isotopes. We find that the width of the elemental distribution (Fig. 7a) is larger than the width expected for a single symmetric fissioning ^{208}Rn. The slight increase of the mean A/Z values of the fragments already mentioned (table 2 and Fig. 9) is pointing again to a series of fissioning parents, the A_0 and A_0/Z_0-ratio of which decrease with the violence of the collision.

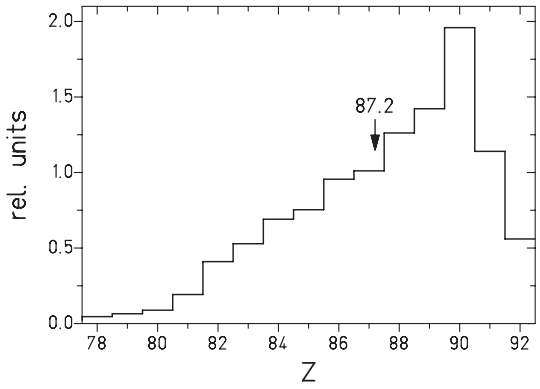

Fig. 11. Calculation of the yield of elements produced by U fragmentation on a Pb target undergoing high energy fission after nuclear interaction [31]

The yields of the many projectile fragments produced in the reaction and undergoing fission should be weighted with the fission probabilities. A distribution of projectile fragments undergoing fission, presented in Fig. 11, has been calculated using a simulation code by courtesy of A. Junghans [31]. This code combines the primary abrasion process [28] with the ablation process including both evaporation and fission. In the simulation, results of fragmentation experiments as well as the most recent theoretical developments are taken into account. Fission delay times [1,8,29], dissipation [32], and collective enhancement of level densities [31] are included in the code. The cross section for low-energy fission, 2.1 b [21], is fully exhausted by the U and Pa isotopes. A fraction of 60% of the fission cross section due to Pa isotopes is estimated to still contribute to high energy fission, and is included in the calculation of the mean value of the atomic number. From the distribution of elements feeding the high energy fission process, Fig. 11, a mean value of 87.2 is found, slightly larger than the measured value Z=85.8. The dotted line of Fig. 7a shows the elemental distribution of fission fragments which is derived when a FWHM of 14.1 charge-units is taken as width for the symmetric fission of each of the fragments [11]. The measured distribution is well reproduced, but the yields of the lightest elements are slightly underestimated. This could indicate that the yields towards lighter fissioning fragments are larger, or more probably, that fission probabilities of those elements are higher.

6 Conclusion

The fission of excited fragments resulting from abrasion-ablation of U-projectiles on a Pb target has been investigated, the signature of fission being given by the velocity distribution of the fragments. For the first time the isotopic yields are extracted for twenty elements around the

region of the symmetric breaking. Between Z=36 and 50, the observed quantities β_f, $\sigma_{\beta\gamma}$, and the Z and N distributions are found compatible with the assumption of a symmetric fission of fragments centered around ^{208}Rn. The small $\overline{N}$ value indicates an energy dissipation significantly larger for this regime than for low-energy fission. Several observations point to the fact, that the very lightest fission fragments (Z < 36) come from lighter fissioning projectile fragmentation products. Contributions from the tails of symmetric fission yields from more abundant heavier projectile fragmentation products alone cannot explain why the yields of light fission fragments are so large. The distribution of fragments which undergo fission, simulated with the code of [28,31] also slightly underestimates the contribution of light Z fragments (Z_0<86). Something in the fission of elements Z_0<86 is not yet fully understood.

A future complete simulation of production of fission fragments from high energy fission and of their kinematics would lead to a more comprehensive explanation. Furthermore, detailed investigations are planned in order to better understand the fragmentation processes of the heaviest nuclei. The fissioning nuclei with N = 126 break into a pair of N = 60 and 6 fission neutrons. Perhaps the fission of spherical closed shell nuclei, not studied until now, has an increased probability and the indication of a peak at $N = (60 \pm 1)$ develops into a solid message, cf. Fig. 7b [13].

References

1. D. Hilscher and H. Rossner: Annales de physique, Vol. **17** (1992) 471
2. G.Friedlander et al.: Phys.Rev.**129** (1963) 1809
3. L. Kowalski, C. Stéphan, H. Langevin-Joliot, P. Radvanyi: Phys. Lett.**2** (1962) 356
4. B. L. Tracy, J. Chaumont, R. Klapisch, J. M. Nitschke, A.M. Postkanzer, E. Roeckl, C. Thibault: Phys. Rev. **C5**, (1972) 222
5. B.N. Belyaev, V.D. Domkin, Yu.G. Korobulin: Nucl. Phys. **A348** (1980) 479.
6. M.de Saint Simon, S.Haan, G.Audi, A.Coc, M.Epherre, P.Guimbal, A.C.Mueller, C.Thibault, F,Touchard, M.Langevin: Phys. Rev. **C26** (1982) 2447
7. M. G. Itkis, V. N. Okolovich, G. N. Smirenkin: Nucl. Phys. **A502** (1989) 243c
8. P. Paul and M. Thoennessen: Ann. Rev. Nucl. Part. Sci. **44** (1994) 65
9. H.-G. Clerc, M. de Jong, T. Brohm, M. Dornik, A. Grewe, E. Hanelt, A. Heinz, A. Junghans, C. Röhl, S. Steinhäuser, B. Voss, C. Ziegler, K.-H. Schmidt, S. Czajkowski, H. Geissel, H. Irnich, A. Magel, G. Münzenberg, F. Nickel, A. Piechaczek, C. Scheidenberger, W. Schwab, K. Sümmerer, W. Trinder, M. Pfützner, B. Blank, A. V. Ignatyuk, G. A. Kudyaev: Nucl. Phys. A 590 (1995) 785
10. K.-H. Schmidt, A. Heinz, H.-G. Clerc, B. Blank, T. Brohm, S. Czajkowski, C. Donzaud, H. Geissel, E. Hanelt, H. Irnich, M.C. Itkis, M. de Jong, A. Junghans, A. Magel, G. Münzenberg, F. Nickel, M. Pfützner, A. Piechaczek, C. Röhl, C. Scheidenberger, W. Schwab, S. Steinhäuser, K. Sümmerer, W. Trinder, B. Voss, C. Ziegler: Phys. Lett. **B325** (1994) 313.
11. S. Steinhäuser, C. Böckstiegel, H.-G. Clerc, A. Grewe, M. de Jong, A. R. Junghans, J. Müller, J. Benlliure, A. Heinz, K.-H. Schmidt and M. Pfützner: Proceedings of the conference on: Dynamical Aspects of Nuclear Fission, Casta Papierniernicka, Slovak republic, Sept 1996, edt. by J. Klimann and B. I. Pustylnik.
12. P. Armbruster, in: Proceedings of 41st Conf. on Chem. Reasarch, The Transactinide Elements, The Welch Foundation, Houston, Texas, 1997
13. A. Heinz, Thesis: Fission Probabilities of Exotic Nuclei, TU Darmstadt, 1998
14. H. Geissel, P. Armbruster, K.-H. Behr, A. Bruenle, K. Burkard, M. Chen, H. Folger, B. Franczak, H. Keller, O. Klepper, B. Langenbeck, F. Nickel, E. Pfeng, M. Pfuetzner, E. Roeckl, K. Rykaczewski, I. Schall, D. Schardt, C. Scheidenberger, K.-H. Schmidt, A. Schroeter, Th. Schwab, K. Suemmerer, M. Weber, G. Muenzenberg, T. Brohm, H.-G. Clerc, M. Fauerbach, J.-J. Gaimard, A. Grewe, E. Hanelt, B. Knoedler, M. Steiner, B. Voss, J. Weckenmann, C. Ziegler, A. Magel, H. Wollnik, J.-P. Dufour, Y. Fujita, D. J. Vieira, B. Sherrill: Nucl. Instrum. Methods **B70** (1992) 286-297
15. A. C. Wahl: Atomic and Nuclear Data Tables 39, 1 (1988)
16. C. Wagemans: The nuclear fission process, edt by CRC press (1991)
17. M. Hesse, M. Bernas, P. Armbruster, T. Aumann, S. Czajkowski, Ph. Dessagne, C. Donzaud, H. Geissel, E. Hanelt, A. Heinz, C. Kozhuharov, Ch. Miehé, G. Münzenberg, M. Pfützner, C. Röhl, K.-H. Schmidt, W. Schwab, C. Stéphan, K. Sümmerer and L. Tassan-Got: Z. Phys. **A355** (1996) 69
18. J. P. Dufour, H. Delagrange, R. Del Moral, A. Fleury, F. Hubert, Y. Llabador, M.B. Mahourat, K.-H. Schmidt: Nucl. Phys. **A387** (1982) 157c.
19. K. Sümmerer, W. Brüchle, D. J. Morrissey, M. Schädel, B. Szweryn, Yang Weifan: Phys. Rev. **C42** (1990) 2546
20. M. Bernas, S. Czajkowski, P. Armbruster, H. Geissel, Ph. Dessagne, C. Donzaud, H.R. Faust, E. Hanelt, A. Heinz, M. Hesse, C. Kozhuharov, Ch. Miehe, G. Münzenberg, M. Pfützner, K.-H. Schmidt, W. Schwab, C. Stephan, K. Sümmerer, L. Tassan-Got, B. Voss: Phys. Lett. **B331** (1994) 19.
21. P. Armbruster, M. Bernas, S. Czajkowski, H. Geissel, T. Aumann, Ph. Dessagne, C. Donzaud, E. Hanelt, A. Heinz, M. Hesse, C. Kozhuharov, Ch. Miehe, G. Muenzenberg, M. Pfuetzner, K.-H. Schmidt, W. Schwab, C. Stephan, K. Suemmerer, L. Tassan-got, B. Voss: Z. Phys. **A355** (1996) 191.
22. C. Donzaud, C. Czajkowski, P. Armbruster, M. Bernas, C. Böckstiegel, Ph. Dessagne, H. Geissel, E. Hanelt, A. Heinz, C. Kozhuharov, Ch. Miehé, G. Münzenberg, M. Pfützner, W. Schwab, C. Stéphan, K. Sümmerer, L. Tassan-Got and B. Voss: to be published in Eur. Phys. Jour. A, 1998
23. J. Benlliure, P. Armbruster, M. Bernas, C. Böckstiegel, S. Czajkowski, C. Donzaud, H. Geissel, A. Heinz, C. Kozhuharov, Ph. Dessagne, G. Münzenberg, M. Pfützner, C. Stéphan, K.-H. Schmidt, K. Sümmerer W. Schwab, L. Tassan-Got and B. Voss: to be published in Eur. Phys. Jour. A, 1998
24. C. Scheidenberger: Thesis, Uni.-Giessen (1995)
25. M. de Jong, A. V. Ignatyuk and K. H. Schmidt: Nucl. Phys. A **613** (1997) 435
26. Th. Schwab: PhD thesis, Universität Giessen, 1992

27. M.L. Justice, Y. Blumenfeld, N. Colonna, D.N. Delis, G. Guarino, K. Hanold, J.C. Meng, G.F. Peaslee, G.J. Wozniak, L.G. Moretto: Phys. Rev. C**49** (1994) R5
28. J.-J. Gaimard and K.-H. Schmidt: Nucl. Phys. **A351** (1991) 709
29. P. Grangé, L. Jun-Qing, H.A. Weidenmüller: Phys. Rev. C **27** (1983) 2063
30. V. E. Viola, Jr. and T. Sikkeland: Phys. Rev. **130** (1963) 2044
31. A.R. Junghans, M. de Jong, H.-G. Clerc, A.V. Ignatyuk, G.A. Kudyaev, and K.-H. Schmidt, Nucl. Phys. **A629**(1998)633
32. H. A. Kramers: Physica 7 (1940) 284
33. M. Bernas, C. Engelmann, P. Armbruster, S. Czajkowski, F. Ameil, C. Böckstiegel, Ph. Dessagne, C. Donzaud, H. Geissel, A. Heinz, Z. Janas, C. Kozhuharov, Ch. Miehé, G. Münzenberg, M. Pfützner, W. Schwab, C. Stéphan, K. Sümmerer, L. Tassan-Got, B. Voss: Phys. Lett B 415 (1997) 111